THE ASTROPHYSICAL JOURNAL, 540:842–850, 2000 September 10

RADIO CONTINUUM EMISSION FROM THE CENTRAL STARS OF M20, AND THE DETECTION OF A NEW SUPERNOVA REMNANT NEAR M20

F. YUSEF-ZADEH
Department of Physics and Astronomy, Northwestern University, Evanston, IL 60208; zadeh@nwu.edu
MARK SHURE[1]
Center for High Angular Resolution Astronomy, Georgia State University, Atlanta, GA 30303; shure@chara.gsu.edu
MARK WARDLE
Research Centre for Theoretical Astrophysics, University of Sydney, Sydney, NSW 2006, Australia; wardle@physics.usyd.edu.au
AND
N. KASSIM
Naval Research Laboratory, Washington, DC 20375-5351; nkassim@shimmer.nrl.navy.mil
Received 1999 October 5; accepted 2000 January 31

ABSTRACT

The Trifid Nebula (M20) is a well-known prominent optical H II region trisected by obscuring dust lanes. Radio continuum VLA observations of this nebula show free-free emission at $\lambda = 3.6$ and 6 cm from three stellar sources lying close to the O7 V star at the center of the nebula. We argue that neutral material associated with these stars is photoionized externally by the UV radiation from the hot central star. We also report the discovery of a barrel-shaped supernova remnant, SNR G7.06−0.12, at the northwest rim of the nebula, and two shell-like features, G6.67−0.42 and G6.83−0.21, adjacent to W28 and M20. We discuss the nature of these features and their possible relationship to the pulsar PSR 1801−2306 and W28 OH (1720 MHz) masers.

Subject headings: galaxies: ISM — H II regions — ISM: individual (Trifid Nebula)

1. INTRODUCTION

The Trifid Nebula (M20), one of the most spectacular optical H II regions in the sky, is centered on a small cluster of hot stars that includes components A–G of HD 164492. M20 is located at a distance of ≈ 1.7 kpc in the Sagittarius spiral arm (but see also Kohoutek, Mayer, & Lorenz 1999); its angular size of 6′ corresponds to about 3 pc at this distance. The ionizing flux of $10^{48.8}$ s^{-1} required to maintain the H II region (Chaisson & Wilson 1975) is supplied by the O7.5 III star HD 164492A (Walborn 1973), which has $M_v = -5.3$ for $A_v \approx 1.3$ toward the central stars (Lynds & O'Neil 1985). This nebula is associated with the young star cluster NGC 6514 and a molecular cloud to the southwest (Ogura & Ishida 1975). The recent detection of several molecular condensations associated with protostellar sources in the H II region and HH 399, a remarkable jetlike structure, suggest a new generation of star formation induced by the nebula (Cernicharo et al. 1998). Hester et al. (1999) have recently shown the high-resolution images of the southeast corner of the nebula based on observations made with WFPC2 of the *Hubble Space Telescope* (*HST*). The emission from this corner of the H II region is dominated by a photoionized photoevaporative flow.

M20 shows many similarities to M42, such as its interaction with its parent molecular cloud and its inhomogeneous nebular structure, but the Trifid is thought to be significantly younger than the Orion Nebula ($\sim 10^5$ yr rather than $\sim 10^6$ yr), and the protostellar molecular condensations associated with massive star formation are even younger (10^4 yr) (Cernicharo et al. 1998).

Here we present near-IR and radio observations of M20. We have detected a number of near-IR stellar sources within the central star cluster in J, H, K, and L images. All seven of the components of HD 164492 (A–G) appear to varying degrees in these images. Three components, B, C, and D, coincide with compact radio continuum sources within 12″ of HD 164492A. These detections suggest that the central massive star is photoionizing the envelope of cool stars in its immediate vicinity similar to the "proplyds" in the Orion Nebula (Churchwell et al. 1987; Garay, Moran, & Reid 1987; O'Dell, Wen, & Hu 1993). Radio images of the nebula at 20 and 6 cm show dark features suggesting the presence of cold and dense regions of dust and gas clouds within the H II region shadowing the UV radiation from HD 164492A. Last, on a scale of tens of arcminutes, we report the discovery of a new candidate barrel-shaped supernova remnant (SNR) lying adjacent to M20 and two shell-type features to the north and east of SNR W28.

2. OBSERVATIONS

The Very Large Array of the National Radio Astronomy Observatory[2] was used in its compact C and D configurations at $\lambda = 20$, 6, and 2 cm in 1987 (Yusef-Zadeh et al. 1991). Follow-up high-resolution observations in the wide BnA array were also carried out at 3.6, 6, and 20 cm in 1998. In all observations 3C 286 was used as standard amplitude calibrator, and 1748−253 and 1730−130 as phase calibrators. The 2 and 6 cm data were successfully self-calibrated in the BnA array configuration. The $\lambda = 20$ cm and 6 cm data corresponding to each configuration were

[1] Visiting Astronomer, NASA Infrared Telescope Facility, which is operated by the University of Hawaii under contract with the National Aeronautics and Space Administration.

[2] The National Radio Astronomy Observatory is a facility of the National Science Foundation, operated under a cooperative agreement by Associated Universities, Inc.

combined before the final images were constructed using VTESS in AIPS. In order to measure the polarization characteristics of G7.06−0.12, we used a different antenna pointing at 6 cm centered at $\alpha(1950)$, $\delta(1950) = 17^h59^m18^s$, $-22°55'45''$, which is offset to the north of the central star HD 164492A.

Wide-field $\lambda = 90$ cm observations toward the supernova remnant W28 which includes M20 were also obtained in the D configuration of the VLA in 1996. In this case 3C 48 and 3C 286 were used as amplitude calibrators, while 1828+487 (3C 380) was used for phase calibration. The 90 cm data were processed using the wide-field imaging task DRAGON present in the NRAO Software Development Environment (SDE) reduction package. DRAGON successfuly completed 5 loops of self-calibration and CLEAN-based deconvolution to generate the final $\lambda = 90$ cm image.

J (1.2 μm), H (1.6 μm), K (2.2 μm), and L (3.5 μm) images were obtained in 1995 July using the near-IR array camera NSFCAM at the NASA Infrared Telescope Facility.[3] Because of the short time spent taking these images, some of the brighter stars were slightly saturated, and stars fill the blank sky images. However, the main results presented here are not affected by the quality of the images.

3. RESULTS AND DISCUSSION

3.1. *Central Stars of M20*

Figure 1 shows contours of 3.6 cm emission with a resolution of 0.″63 × 0.″45 (P.A. = 80°) with rms ≈33 μJy. Radio continuum peaks whose flux densities and sizes are listed in Table 1 coincide with the positions of HD 164492B, C, and D. Optical positions of HD 164492A, B, and C are also listed in Table 1 using the *Hipparcos* coordinates, which are based on a fit to a multiple-source model. The quality of the model solution for "C" using the *Hipparcos* database was poor, so we did not include it. However, there is an excellent agreement between the absolute position of radio and optical sources to within 0.″1, especially for sources B and C.

The gray-scale images in Figure 2 show the components of the multiple star HD 164492 and are identified on the J image, which is very similar to visible images. The central star A coincides with the optical star HD 164992A but is not detected at a level of rms ≈33 μJy at 3.6 cm. Source C, the brightest radio source, has a flux of 2.43 mJy at 3.6 cm. HD 164492D lies only 2″ west of star C and was found to be a strong Hα emission source by Herbig, who classified it as a Be star and named it LkHα 123 (Herbig 1957). It was also included as Hα emission star 46 in a survey by Velge (1957), and star 145 in the survey of Ogura & Ishida (1975). The D star is the brightest point source in recent 12.5 and 17.9 μm images that were taken with the JPL MIRLIN camera at the IRTF (M. E. Ressler & M. Shure 1995, private communication). Notice several objects in the L image that are either unseen or are very much dimmer shortward of K. Among these newly discovered sources is one roughly 3″ northeast and the other only 2″ north of star A. If they are

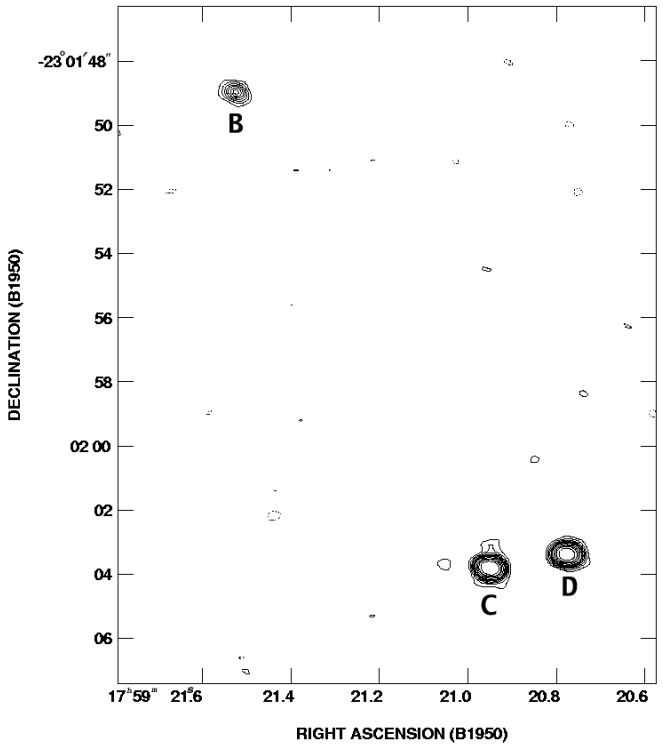

FIG. 1.—Contours of total intensity at $\lambda = 3.6$ cm with a spatial resolution of 0.″63 × 0.″45 (P.A. = 80°) and an rms noise of 33 μJy. The levels are set at −3, 3, 5, 7, 9, 11, 13, 15, 20, 25, 30, and 40 times the rms noise.

[3] The NASA Infrared Telescope Facility is operated under contract by the University of Hawaii.

TABLE 1

VLA AND *Hipparcos* POSITIONS OF M20 STARS

SOURCE DESIGNATION	α_{1950}	δ_{1950}	S_p (mJy)	DECONVOLVED SIZE		
				Major (arcsec)	Minor (arcsec)	P.A. (deg)
M20-VLA-B.....	17 59 21.52±1E−3	−23 01 48.98±1E−2	0.61	...	...	...
M20-VLA-C.....	17 59 20.95±3E−4	−23 02 03.8±3E−3	2.46	...	...	...
M20-VLA-D	17 59 20.78±3E−4	−23 02 03.38±3E−3	2.24	0.19±0.03	0.12±0.06	129±27
M20-HIP-A	17 59 21.38	−23 01 54.8	...	...	...	...
M20-HIP-B	17 59 21.53	−23 01 48.9	...	...	...	...
M20-HIP-C	17 59 20.96	−23 01 03.8	...	...	...	...

NOTE.—Units of right ascension are hours, minutes, and seconds, and units of declination are degrees, arcminutes, and arcseconds.

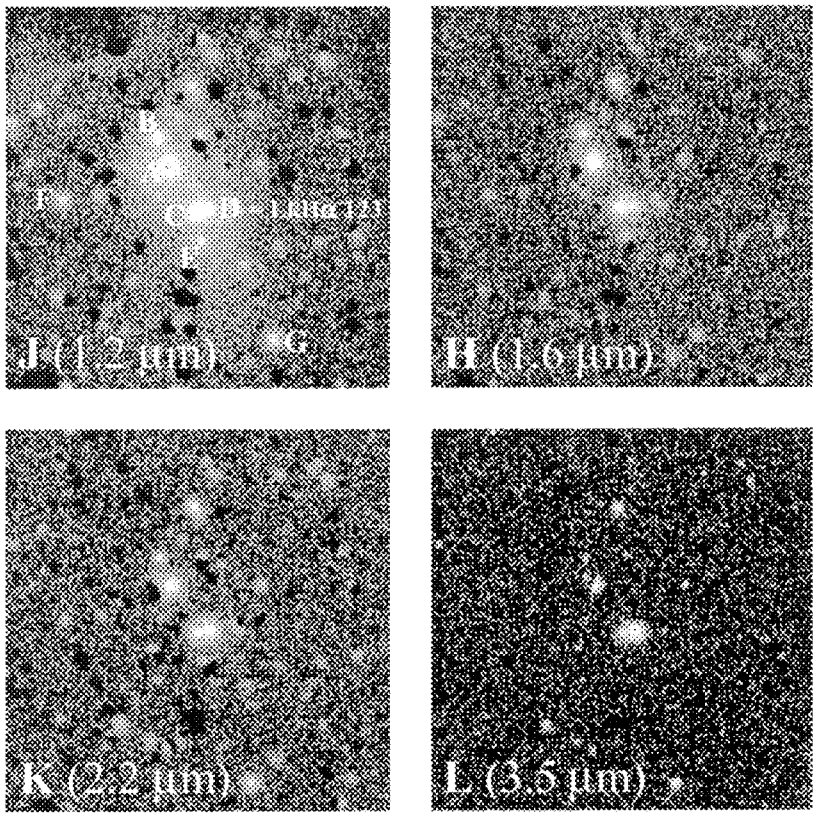

FIG. 2.—Exploratory NSFCAM images (log-scaled) of the central cluster of M20. The visible components of the multiple star HD 164492 are labeled in the *J* image. The field of each image is approximately 80″ × 80″, with north up and east to the left. The dark spots are due to stars in the nearby blank-sky image which is used to subtract the background.

physically associated with this star (2″ = 3400 AU at 1.7 kpc), they would represent some of the first low-mass companions to high-mass stars.

All three sources B, C, and D are also detected at 6 cm based on our high-resolution BnA array data. Accurate spectral index measurements between 6 and 3.6 cm using similar *uv* coverage and spatial resolution of 0.″99 × 0.″7 (P.A. = −87°) showed $\alpha \approx 0$ for sources B and C and $\alpha = -0.19$, where $F_\nu \propto \nu^\alpha$, for source D. The D star as listed in Table 1 is the only star resolved in our 3.6 cm measurements with a deconvolved size of 0.″19 × 0.″12 (P.A. = 129°).

3.2. *Dense Neutral Gas Associated with Stars B, C, and D*

What is the origin of the emission from B, C, and D? By analogy with the Orion Nebula, one suspects that these sources are externally ionized neutral condensations being photoevaporated by the intense UV field of the O7.5 III star HD 164492A. The argument that this is so proceeds similarly to those of Garay et al. (1987) that Churchwell et al. (1987) applied to the proplyds first detected in radio continuum in the Orion Nebula.

The flat spectra of sources B, C, and D indicate that their radio continuum arises from optically thin free-free emission. For $T \approx 8000$ K, the volume emission measures are $n_e^2 V \sim 1 \times 10^{57}$ cm^{-3}, and for the emission to be optically thin the characteristic scale R of the emission region $\gtrsim 50$ AU. If this region is a roughly constant-density compact H II region, this scale represents the outer boundary. However, the gas is then gravitationally unbound to the central star and the H II region would expand on a timescale of ∼30 yr. On the other hand, if the emitting region is an ionized wind with $n_e \propto r^{-2}$, the emission is dominated by the innermost radii and R corresponds to the *inner* boundary. An ionized stellar wind can be discounted, because then $R \ll 50$ AU, and the mix of optically thin and optically thick contributions at any given frequency produces a $\nu^{0.6}$ spectrum; further, the source would be much weaker than observed. Thus we conclude that the emitting region is an ionized wind that is photoevaporated from a reservoir of neutral material near the star.

The neutral reservoir cannot be too large, as sources B and C are unresolved and source D is barely resolved. Adopting a distance of 1.7 kpc to M20, the geometric mean of the semimajor and semiminor axes of source D (see Table 1) is $R \approx 130$ AU, and the corresponding upper limit on sources B and C is 80 AU. The neutral reservoir will be even smaller, and is therefore clearly associated with the star.

The O7.5 III star HD 164492A is likely to be the dominant source of the ionizing photons. An O7.5 III star emits 9.6×10^{49} ionizing photons s^{-1} (Panagia 1973), so that the total ionizing flux incident on a 130 AU radius target at the projected distance of star D (≈0.095 pc) is 1.1×10^{45} s^{-1}. This is comparable to the hydrogen recombination rate of source D, 6.6×10^{44} s^{-1}. The recombinations in sources B and C are also consistent with this hypothesis. Note, however, that stars HD 164492B, C, and D are of spectral type B (Kohoutek et al. 1999) and produce $\sim 10^{45}$ Lyman continuum photons or more per second, so they may contribute significantly to the ionization if enough photons can intercept the nearby neutral material.

Our observations do not determine the distribution of the neutral material associated with stars B, C, and D, but we speculate that it is in circumstellar disks, as for the "proplyds" in Orion.

3.3. *Embedded East-West Dust Lane in M20*

A $\lambda = 6$ cm gray-scale image with resolution of $2\farcs3 \times 1\farcs1$ (P.A. $= -80°$) and an optical image based on the Palomar Sky Survey are compared in Figures 3*a* and 3*b*. The prominent elongated dust lanes to the southwest, southeast, and northwest of the optical image have no counterpart in radio, indicating that these dust features lie in front of the H II region. However, there is a remarkable east-west dark radio feature that closely mimics the shape of the optical dust lane seen to the southwest of the central hot star in Figure 3*b* near $\alpha, \delta(1950) = 17^h59^m17^s, -23°02'50''$. Figure 4 shows a north-south slice cut across this feature in the 6 cm radio image. The radio continuum emission is depressed by a factor of 3 where the optical nebula appears to be crossed by an east-west dark dust lane with a thickness of about $40''$ (0.3 pc). The correlation between reduced radio emissivity and the optical dust lane is evidence for the dust lane being embedded within the nebula. Other examples of dark features are also apparent in the inhomogeneous large-scale distribution of ionized gas beyond the inner region shown in Figure 3. These dark features are particularly noticeable as broken shell-like structures surrounding the $6'$ size of the nebula, and correlate with the distribution of the HCO^+ $J = 1$–0 emission from the nebula presented by Cernicharo et al. (1998). We also note a column of dark features labeled as dark shadow within the nebula to the east of TC1. These dark features are unlikely to be produced by a lack of short *uv* spacing data but are instead due to a dense 10^4 cm^{-3} column of gas arising from the surface layer of the molecular cloud and causing the H II region to become ionization-bounded. The dearth of emission from a

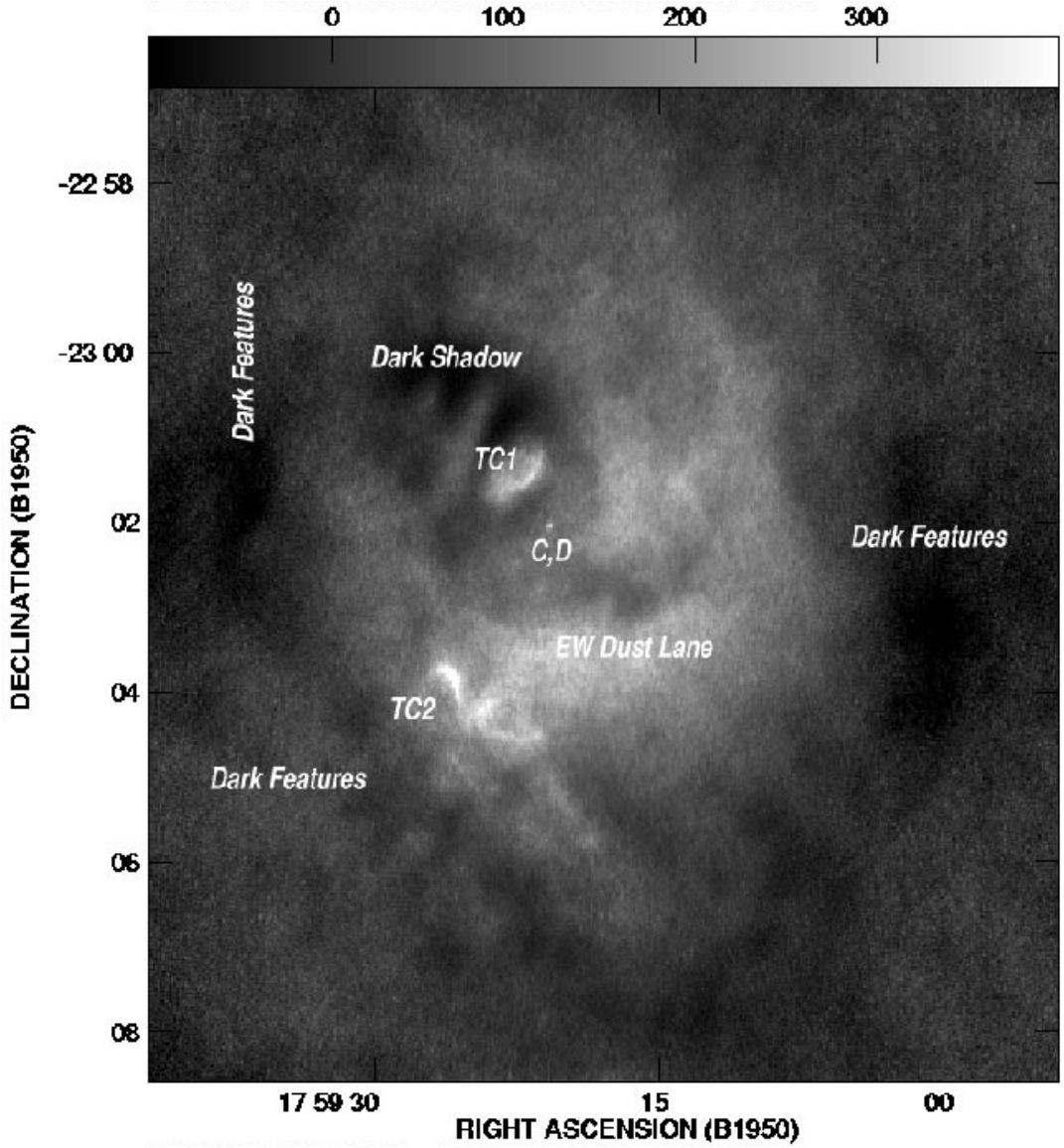

FIG. 3*a*

FIG. 3.—A $\lambda = 6$ cm radio continuum image (*a*) with a resolution of $2\farcs3 \times 1\farcs1$ (P.A. $= -8°$) is shown against a Palomar image from the Digital Sky Survey (*b*). The two images show an identical region, and prominent features are identified in both images. In (*a*) the gray-scale flux range is between -100 and 400 μJy beam^{-1}; in (*b*) it is between 2.000 and 9.000.

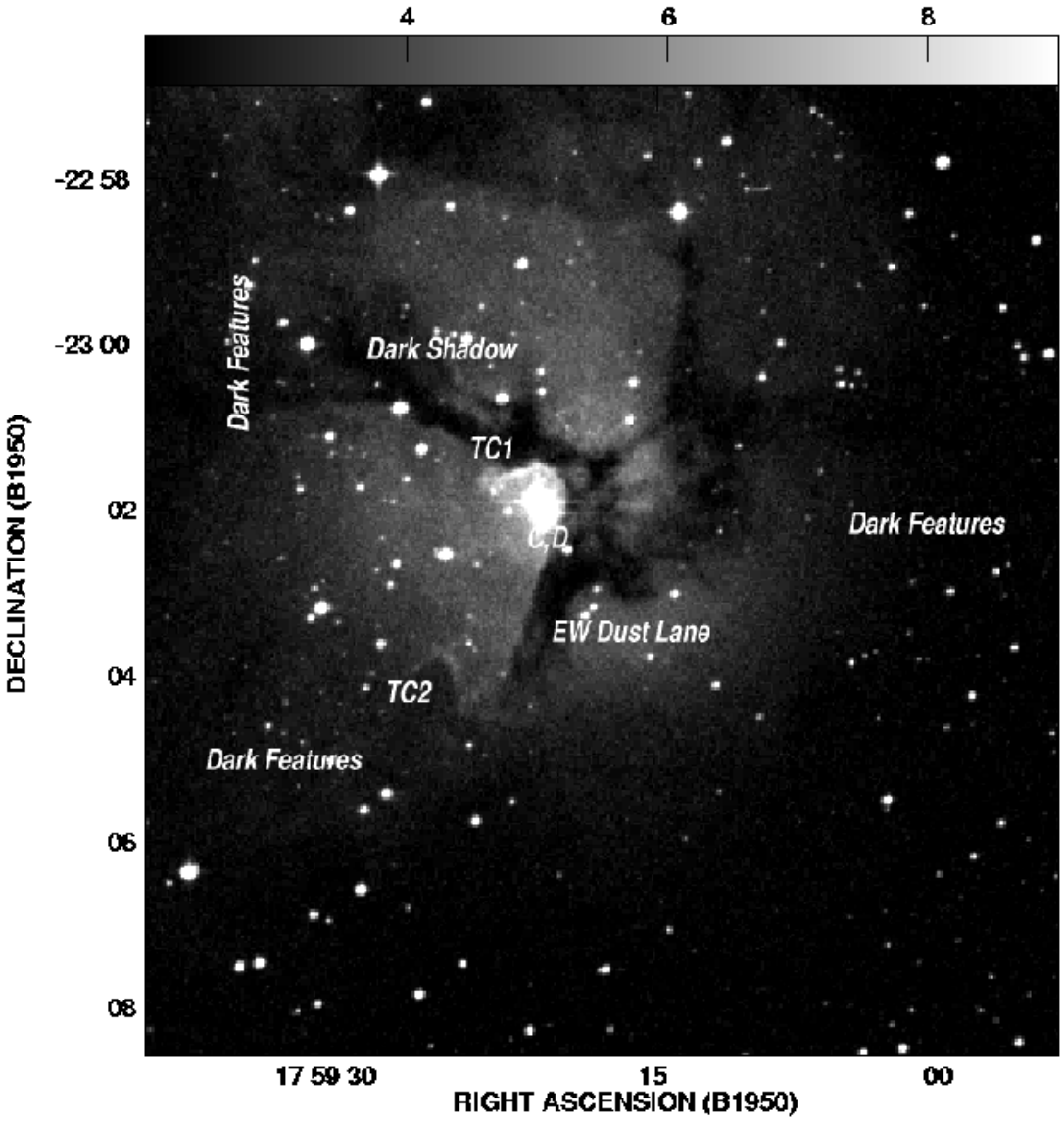

FIG. 3*b*

series of dark features including the east-west feature, as best represented in Figure 3*a*, is interpreted to correspond to the peaks of dense gas shielding the ionizing flux arising from the central hot star. These columns of dense gas are responsible to reduce the emission measure $n_e^2 L$, where n_e and L are the electron density and the path length.

3.4. *Ionized Rims of TC1 and TC2*

Figure 5 shows total intensity contours over the central part of the H II region at $2''.3 \times 1''.1$ resolution (P.A. $= -80°$). The two extended ionized features to the northwest and southeast are associated with two bright pointlike condensations of dust emission at 1.3 mm denoted TC1 and TC2 by Cernicharo et al. (1998). High-velocity broad wings in the HCO^+ emission from TC1 and a jetlike HH feature associated with TC2 led Cernicharo et al. to suggest that these condensations are associated with protostars. The ages of these condensations are estimated to be about 10^4 yr and therefore formed after the birth of the H II region. The extended photoionized features in Figure 5 delineate the ionized rims of TC1 and TC2 facing the central hot star. High-resolution WFPC2 observations of TC2 using a number of spectral lines was recently reported by Hester et al. (1999), who interpret the ionized layer of TC2 as a photoionizing photoevaporative flow. The typical flux density of the ionized rims of TC1 and TC2 is about 0.5 mJy beam^{-1}, which corresponds to $n_e \approx 2 \times 10^3$ cm^{-3}.

4. DISCOVERY OF A SUPERNOVA REMNANT AND TWO SHELL-LIKE FEATURES

4.1. *G7.06−0.12: A Barrel-shaped SNR*

Figure 6 shows a large-scale gray-scale image of M20 and its immediate vicinity at 20 cm (D array only) with a resolution of $59''.1 \times 33''.7$ (P.A. $= -2°$). We note the prominent W28 SNR to the southwest and report here a newly discovered shell-type SNR, G7.06−0.12, with a diameter of $13'$ adjacent to the northwest rim of M20. Radio continuum measurements at 6 cm show linearly polarized emission at the northern rim of M20 near $\alpha(1950)$, $\delta(1950) = 17^h59^m22^s$, $-22°55'$. The degree of polarization is about 28% at 6 cm based on D-array data with a resolution of $29''.8 \times 14''.3$ (P.A. $= -27°$). This radio source has no obvious optical

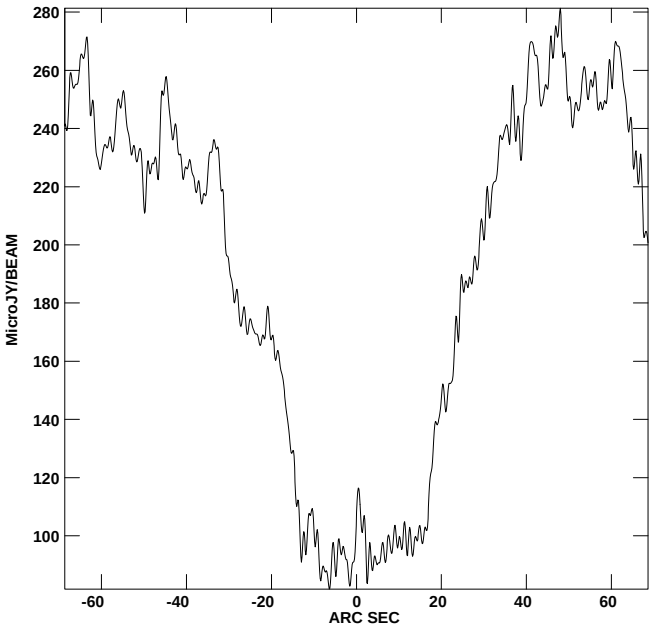

FIG. 4.—A slice cut along the east-west dust lane at 6 cm centered at $\alpha(1950), \delta(1950) = 17^h59^m17^s, -23°02'49''.5$ at the position angle of 178°.

counterpart and is a previously uncataloged, synchrotron-emitting SNR.

Further evidence that G7.06−0.12 is a SNR is provided by its morphology, revealed in the contour map of the 20 cm image centered on the remnant and displayed in Figure 7. Here G7.06−0.12 is revealed as a classic barrel-shaped SNR aligned roughly with its major axis parallel to the Galactic equator (Gaensler 1998). The western rim of the barrel is more extensive and is about 3–4 times brighter than the eastern rim, which protrudes north of M20 near $\alpha = 17^h59^m25^s$. We also note several clumps of 20 cm continuum features to the north of G7.1−0.1 and a 8′ elongated structure running north-south toward the center of the SNR.

Finally, the identification of G7.06−0.12 as a barrel-shaped SNR is confirmed by its nonthermal continuum spectrum and morphology as determined from complementary 90 cm observations. Figure 8 is a D-array 90 cm contour image centered on the bright SNR W28 with an angular resolution of 5′.5 × 2′.6 (P.A. = 13°.4). Protruding north of the W28 SNR near $\alpha = 17^h58^m.5$ is the western half of G7.06−0.12, whose eastern half is now smothered by M20 centered near $\alpha = 17^h59^m.3$. G7.06−0.12's barrel-shaped morphology is also revealed on reinspection of the higher resolution (∼20′) wide-field 90 cm image centered near the SNR G5.4−0.1 (Frail, Kassim, & Weiler 1994). The 90 cm image is dominated by W28, whose integrated flux is 350 ± 50 Jy.

Confirmation of the nonthermal spectrum of G7.06−0.12 comes from comparing the integrated flux of the well-defined western half of the barrel, giving an average of ∼3.9 Jy as obtained from the two 90 cm measurements and ∼1.9 Jy from the 20 cm image. This yields the canonical $\alpha \sim -0.5 \pm 0.15$ nonthermal spectrum of a typical shell-type SNR, as expected. The images are sufficient to confirm that the eastern half of G7.06−0.12 is also nonthermal, but higher resolution 90 cm data are required to determine the spectrum of either side of the barrel more accurately than this. It is interesting to note that the integrated flux of M20 from our D-array 90 cm map, which includes some flux from the eastern half of G7.06−0.12, is 11 ± 2 Jy. Together with the 14 ± 3 Jy integrated flux present on our 20 cm map, this indicates a slightly inverted spectrum revealing that the H II region has started to become optically thick at 90 cm as is common.

While the eastern rim of G7.06−0.12 merges with the northwest segment of M20, there is no morphological evidence for the interaction of the SNR and M20. We cannot rely on the Σ-*D* relationship to estimate the distance to G7.06−0.12 (Green 1991), but VLA observations at 74 MHz should be able to determine the relative positions, since at that frequency M20 would have become completely optically thick and it would be apparent whether the eastern side of the barrel was being absorbed or not. We note that this region of the Galaxy is rich in having a number of H II complexes (M8, M20), the SNR W28 expanding into an adjacent molecular cloud (e.g., Wootten 1981) as well as a young star cluster, NGC 6514. Thus, it is plausible that SNR G7.06−0.12 is associated with the young cluster, but further studies are needed.

4.2. *G6.67−0.42: A Nonthermal Shell-Type Feature*

An additional new radio continuum source identified in this rich region of the Galaxy is G6.67−0.42, located 20′ south of M20 as labeled in Figure 6. G6.67−0.42 is clearly distinct from W28 and shows a protruding feature in the eastern part of W28 near $\delta(1950) = -23°23'$. This feature, which is curving convex downward, is another previously unidentified source. Its morphology is clearly shell-like, as indicated from the 20 cm image displayed in Figure 7. However, the limitation of the 20 cm field of view together with the confusion from W28 allows only a northeastern fragment of an apparently circular shell to be clearly delineated. High-resolution observations at 20 cm reveal this new feature, which otherwise would have been associated with W28 in earlier low-resolution measurements. The 90 cm image shown in Figure 8 shows G6.67−0.42 merged with the eastern part of the shell in W28.

Estimating the spectrum of G6.67−0.42 was done by convolving the 20 and 90 cm images to the same resolution, 328″.8 × 157″.6. The spectrum is estimated to be $\approx -0.35 \pm 0.15$ from the peak flux and integrated flux of the shell fragment at 20 and 90 cm. The nonthermal emission could be supplied or be part of the W28 remnant itself, e.g., resulting from a so-called "blowout" where the main blast wave has encountered a lower density ISM region. However, the geometry of the weaker shell-like feature and its distinct structure from W28 is not classic blowout morphology in that its implied center of curvature is significantly different from that of the main W28 shell. Future observations should clarify whether the nonthermal shell fragment is either part of W20 or yet another previously unidentified shell-type SNR.

4.3. *G6.83−0.21: A Shell-Type Structure*

Last, we detect a weakly emitting shell-like source G6.83−0.21 lying between M20 and W28, as labeled in Figure 6. This source lies in a difficult region of our 20 cm image where a "negative bowl" surrounding both W28 and M20 suppresses any emission arising from this weak source. In spite of this difficulty, we note a shell source with a diameter of about 15′ lying between the northern and southern edges of W28 and G7.06−0.12, respectively. The

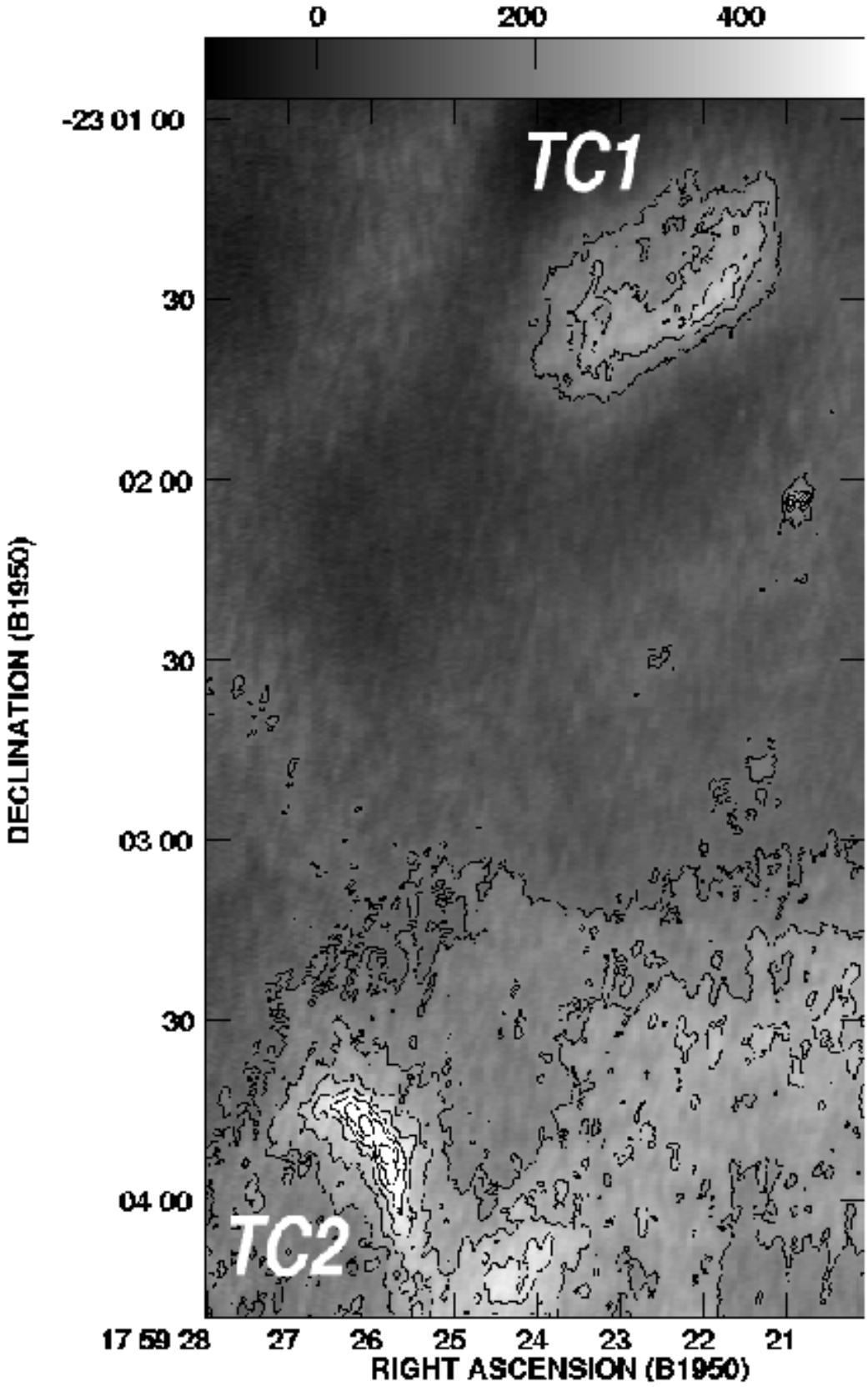

FIG. 5.—Closeup view of Fig. 3*a* showing TC1 and TC2 regions with contour levels set at -4, 4, 6, 8, 10, 12, 14, and 16 times 40 μJy beam^{-1}

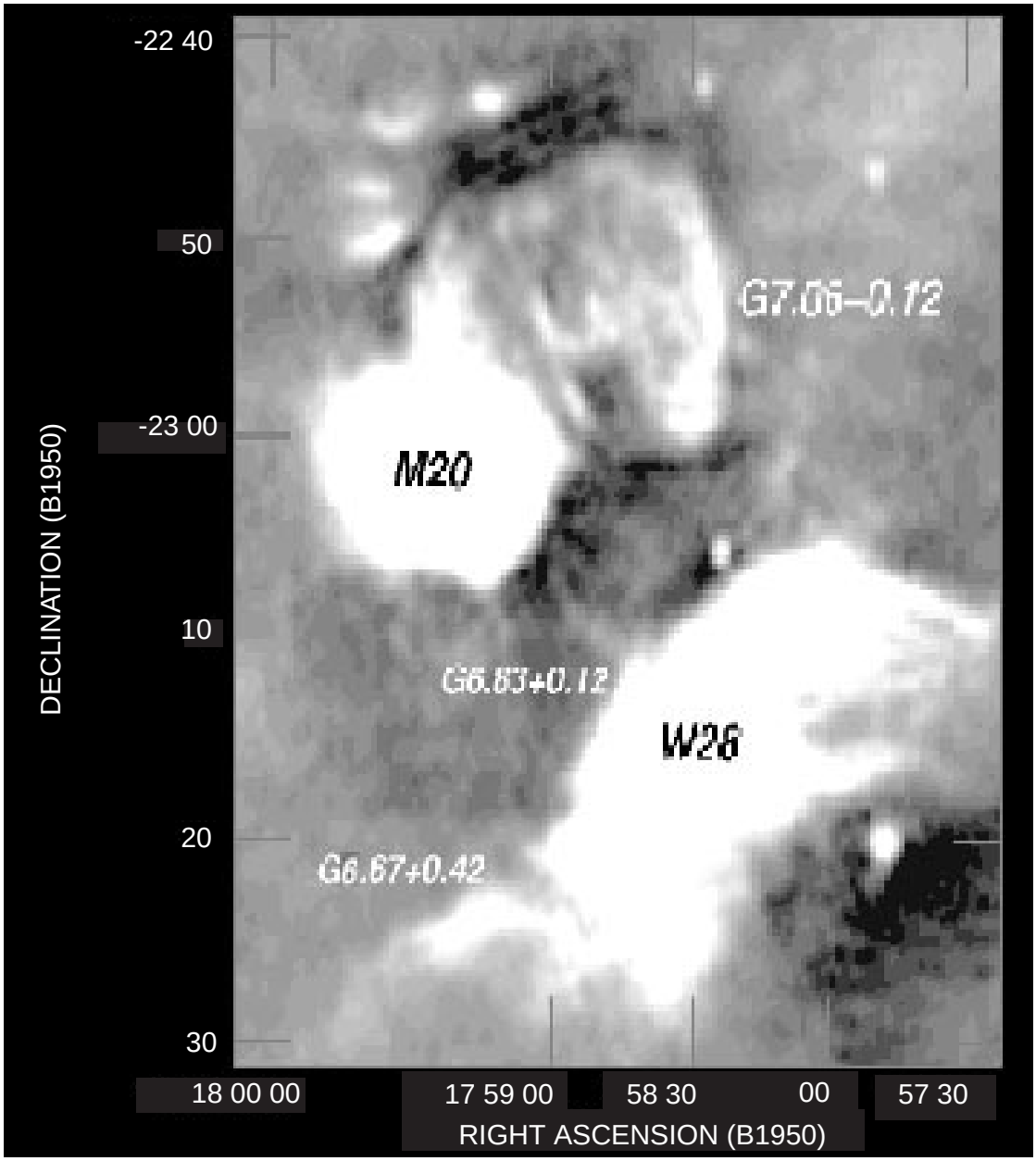

FIG. 6.—Gray-scale image of the M20 region $\lambda = 20$ cm with a spatial resolution of 65″.2 × 39″.3 (P.A. = −34°) identifying prominent sources. The primary-beam correction has not been applied to this image.

eastern edge of G6.83−0.21 is brighter and has a typical flux density of about 4 mJy beam^{-1} above the negative depression at a level of −6 mJy beam^{-1}.

It is difficult to determine the nature of G6.83−0.21 because of the lack of spectral and polarization information. However, two observational anomalies, described below, imply that G6.83−0.21 is possibly a distinct shell-type SNR. The bright compact source G6.833−0.093 and the pulsar PSR 1758−23 lie at the geometrical center of the shell source G6.83−0.21. An association between PSR 1758−23 and the W28 SNR has been suggested on the basis of age, even though the pulsar lies outside the W28 shell. This hypothesis has the difficulty that it has a much larger dispersion measure than would be expected if the pulsar were placed 2 kpc away (Kaspi et al. 1993), although Frail, Kulkarni, & Vasisht (1993) have argued that the large dispersion and scattering of the pulses from PSR 1758−23 are caused by a dense screen of ionized gas located along the line of sight. Another anomaly is the kinematics of the OH (1720 MHz) masers observed across the northern part of W28 (Claussen et al. 1997). OH (1720 MHz) masers have recently been identified as a signature of SNRs interacting with molecular clouds (e.g., Frail, Goss, & Slysh 1994; Lockett, Gauthier, & Elitzur 1999; Wardle 1999). The kinematics of these masers are generally found to be similar to the systemic velocity of molecular clouds into which SNRs are expanding. Claussen et al. (1997), however, notice an exception in W28, where the masers fall into low- and high-velocity groups. Two molecular clouds have been observed toward W28 at 7 and 17 km s^{-1} in various molecular lines (Wootten 1981). To explain this velocity difference, Claussen et al. (1997) suggest that the entire low-velocity molecular cloud has been accelerated by the SNR shock along our line of sight.

The above anomalies may be resolved if G6.83−0.21 is a shell-type SNR associated with the PSR 1758−23 and is

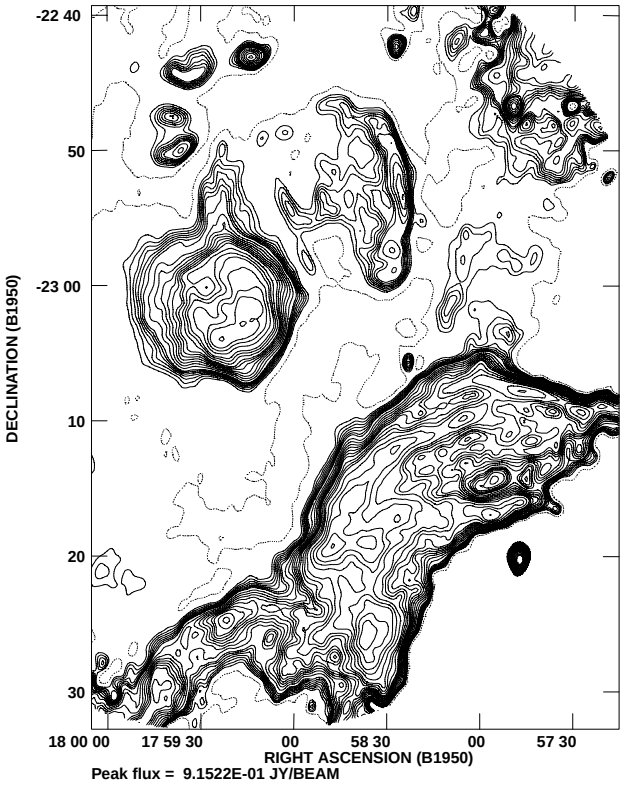

FIG. 7.—Contours of total intensity at $\lambda = 20$ cm with a spatial resolution of 65.″2 × 39.″3 (P.A. = −34°) with an rms noise of 1 mJy. The levels are set at −3, 3, 5, 7, 9, 11, 13, 15, 20, 25, 30, 35, 40, 45, 50, 60, 70, 80, 100, 120, 140, 170, 200, 250, 300, and 350 times 2 mJy beam^{-1}.

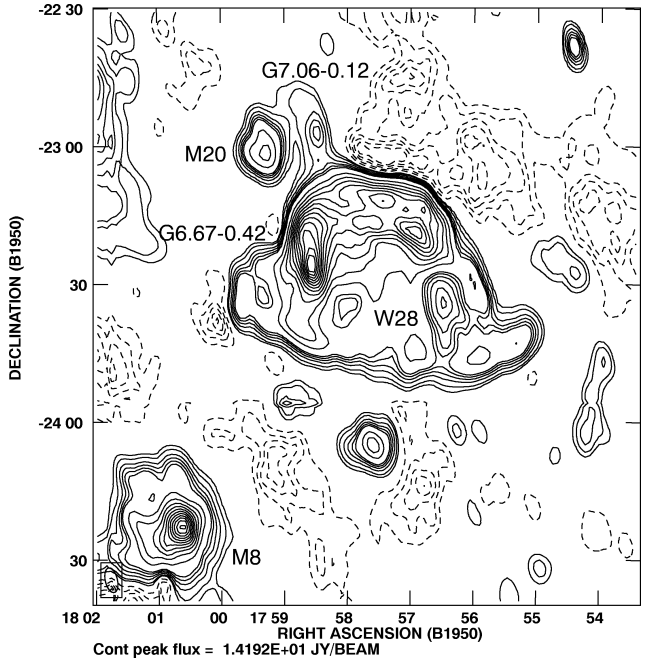

FIG. 8.—Contours of $\lambda = 90$ cm emission obtained from the D-array configuration of the VLA. The angular resolution is 5.″5 × 2.″6(P.A. = 13.°4), and the rms noise is about 200 mJy beam^{-1}. The peak emission is 14.2 Jy beam^{-1}, and contour levels are at 100 mJy beam^{-1} × −8, −6, −4, −2, −1, 1, 2, 4, 6, 8, 10, 20, 30, 40, 50, 60, 70, 80, 90, 100, 110, 120, and 130.

interacting with a distinct 7 km s^{-1} molecular cloud. The distance to G6.83−0.21 is difficult to estimate, but it has to be placed at a larger distance than 2 kpc to be consistent with the high dispersion of pulsar signals. Future observations of G6.83−0.21 should be important to clarify whether this feature is a confusing source in this complex region of the Galaxy or whether it is a new member of the class of SNRs with associated OH (1720 MHz) masers lying within the inner several degrees of the Galactic center (Yusef-Zadeh et al. 1999).

F. Yusef-Zadeh's work was supported in part by NASA. Basic research in radio astronomy at the Naval Research Laboratory is supported by the Office of Naval Research.

REFERENCES

Cernicharo, J., et al. 1998, Science, 282, 462
Chaisson, E. J., & Wilson, R. F. 1975, ApJ, 199, 647
Churchwell, E., Wood, D. O. S., Felli, M., & Massi, M. 1987, ApJ, 321, 516
Claussen, M. J., Frail, D. A., Goss, W. M., & Gaume, R. A. 1997, ApJ, 489, 143
Frail, D. A., Goss, M. W., & Slysh, V. I. 1994, ApJ, 424, L111
Frail, D. A., Kassim, N. E., & Weiler, K. W. 1994, ApJ, 107, 1120
Frail, D. A., Kulkarni, S. R., & Vasisht, G. 1993, Nature, 365, 136
Gaensler, B. M. 1998, ApJ, 493, 781
Garay, G., Moran, J. M., & Reid, M. J. 1987, ApJ, 314, 535
Green, A. D. 1991, PASP, 103, 209
Herbig, G. H. 1957, ApJ, 125, 654
Hester, J., Scowen, P., Stappelfeldt, K., & Krist, J. 1999, BAAS, 194, 68.10
Kaspi, V. M., Lyne, A. G., Manchester, R. N., Johnston, S., D'Amico, N., & Shemar, S. L. ApJ, 1993, 409, L57
Kohoutek, L., Mayer, P., & Lorenz, R. 1999, A&AS, 134, 129
Lockett, P., Gauthier, E., & Elitzur, M. 1999, ApJ, 511, 235
Lynds, B. T., & O'Neil, E. J., Jr. 1985, ApJ, 294, 578
O'Dell, C. R., Wen, Z., & Hu, X. 1993, ApJ, 410, 696
Ogura, K., & Ishida, K. 1975, PASJ, 27, 119
Panagia, N. 1973, AJ, 78, 929
Velghe, A. G. 1957, ApJ, 126, 302
Walborn, N. R. 1973, AJ, 78, 1067
Wardle, M. 1999, ApJ, 525, L101
Wootten, A. 1981, ApJ, 245, 105
Yusef-Zadeh, F., Goss, W. M., Roberts, D. A., Robinson, B., & Frail, D. A. 1999, ApJ, 527, 172
Yusef-Zadeh, F., Reiss, D. J., Hollis, J. M., & Klinglesmith, D. A. 1991, BAAS, 23, 1364